

Vehicle Detection in Aerial Images

Michael Ying Yang^a, Wentong Liao^b, Xinbo Li^b, Bodo Rosenhahn^b

^a*ITC Faculty of Geo-Information Science and Earth Observation, University of Twente*

^b*Institute of Information Processing, Leibniz University Hannover*

Abstract

The detection of vehicles in aerial images is widely applied in many applications. Comparing with object detection in the ground view images, vehicle detection in aerial images remains a challenging problem because of small vehicle size, monotone appearance and the complex background. In this paper, we propose a novel double focal loss convolutional neural network framework (DFL-CNN). In the proposed framework, the skip connection is used in the CNN structure to enhance the feature learning. Also, the focal loss function is used to substitute for conventional cross entropy loss function in both of the region proposed network and the final classifier. We further introduce the first large-scale vehicle detection dataset ITCVD with ground truth annotations for all the vehicles in the scene. We demonstrate the performance of our model on the existing benchmark DLR 3K dataset as well as the ITCVD dataset. The experimental results show that our DFL-CNN outperforms the baselines on vehicle detection.

Keywords: object detection, aerial images, convolutional neural network (CNN), focal loss function

1. Introduction

The detection of vehicles in aerial images is widely applied in many applications, *e.g.* traffic monitoring, vehicle tracking for security purpose, parking lot analysis and planning, *etc.* Therefore, this topic has caught increasing attention in both academic and industrial fields (Gleason et al., 2011; Liu and Mattyus, 2015;

*Corresponding author. Tel.: +31 53 489 2916; fax: +31 53 487 4335.

Email addresses: michael.yang@utwente.nl (Michael Ying Yang),
liao@tnt.uni-hannover.de (Wentong Liao), xinbo@tnt.uni-hannover.de (Xinbo Li),
rosenhahn@tnt.uni-hannover.de (Bodo Rosenhahn)

Chen et al., 2016). However, compared with object detection in ground view images, vehicle detection in aerial images has a lot of different challenges, such as much smaller scale, complex backgrounds and the monotonic appearance. See Figure 1 for an illustration.

Before the emergence of deep learning, hand-crafted features combined with a classifier are the mostly adopted ideas to detect vehicles in aerial images (Zhao and Nevatia, 2003; Gleason et al., 2011; Liu and Mattyus, 2015). However, the hand-crafted features lack generalization ability, and the adopted classifiers need to be modified to adapt the of the features. Some previous works also attempted to use shallow neural network (LeCun et al., 1990) to learn the features specifically for vehicle detection in aerial images (Cheng et al., 2012; Chen et al., 2014). However, the representational power of the extracted features are insufficient and the performance meets the bottleneck. Furthermore, all of these methods localize vehicle candidates by sliding window search. It's low efficient and leads to costly and redundant computation. The window's sizes and sliding steps must be carefully chosen to adapt the varieties of objects of interest in dataset.

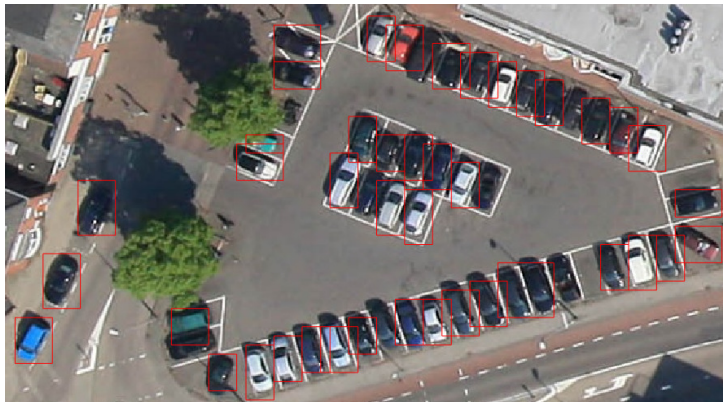


Figure 1: Vehicles detection results on the proposed dataset.

In recent years, deep convolutional neural network (DCNN) has achieved great successes in different tasks, especially for object detection and classification classification (Krizhevsky et al., 2012; LeCun et al., 2015). In particular, the series of methods based on region convolutional neural network (R-CNN) (Girshick et al., 2014; Girshick, 2015; Ren et al., 2015) push forward the progress of object detection significantly. Especially, Faster-RCNN (Ren et al., 2015) proposes the region proposal network (RPN) to localize possible object instead of traditional sliding window search methods and achieves the state-of-the-art performance in

different datasets in terms of accuracy. However, these existing state-of-the-art detectors cannot be directly applied to detect vehicles in aerial images, due to the different characteristics of ground view images and aerial view images (Xia et al., 2017). The appearance of the vehicles are monotone, as shown in Figure 1. It’s difficult to learn and extract representative features to distinguish them from other objects. Particularly, in the dense park lot, it is hard to separate individual vehicles. Moreover, the background in the aerial images are much more complex than the nature scene images. For examples, the windows on the facades or the special structures on the roof, these background objects confuse the detectors and classifiers. Furthermore, compared to the vehicle sizes in ground view images, the vehicles in the aerial images are much smaller (ca. 50×50 pixels) while the images have very high resolution (normally larger than 5000×2000 pixels). Lastly, large-scale and well annotated dataset is required to train a well performed DCNN methods. However, there is no public large-scale dataset such as ImageNet (Deng et al., 2009) or ActivityNet (Caba Heilbron et al., 2015), for vehicle detection in aerial images.

To address these problems, we propose a specific framework for vehicle detection in aerial images, as shown in Figure 2. The novel framework is called double focal loss convolutional neural network (DFL-CNN), which consists of three main parts: 1) A skip-connection from the low layer to the high layer is added to learn features which contains rich detail information. 2) Focal loss function (Lin et al., 2017) is adopted in the RPN instead of traditional cross entropy. This modification aims at the class imbalance problem when RPN determine whether a proposal is likely an object of interest. 3) Focal loss function replaces the cross entropy in the classifier. It’s used to handle the problem of easy positive examples and hard negative examples during training. Furthermore, we introduce a novel large-scale and well annotated dataset for quantitative vehicle detection evaluation - ITCVD. Towards this goal, we collected 173 images with 29088 vehicles, where each vehicle in the ITCVD dataset is manually annotated using a bounding box. The performance of the proposed method is demonstrated with respect to a representative set of state-of-the-art baselines, leveraging the proposed ITCVD dataset and DLR 3K dataset (Liu and Mattyus, 2015). We make our code and dataset online available.

2. Related Work

Object detection and classification have been the central topics in the computer vision and photogrammetry literature. Most of the existing methods can be

roughly divided into three main steps: candidate region proposal, feature extraction and classification.

To generate the regions which likely contains the object of interest, many methods employ sliding-window search strategy (Felzenszwalb et al., 2010; Liu and Mattyus, 2015; Chen et al., 2016). These methods used windows with varied scales and ration to scan through the image with fixed step size. Sliding-window search strategy has high computation and time complexity, and most of the windows are redundant. Uijlings et al. (2013) proposed the algorithm dubbed *Selective Search* to generate possible object locations. This method combines the merits of both an exhaustive search and segmentation. It's widely adopted to combine with DCNN methods for object detection, such as Girshick et al. (2014); Girshick (2015). Ren et al. (2015) proposed the *region proposal network* (RPN) and then became the most popular method for region proposal.

Before classification, features are extracted within each region candidate. Kembhavi et al. (2011) used SIFT features for vehicle detection. Gleason et al. (2011); Han et al. (2006) employed HoG features, while Bai et al. (2006) adopted Haar-like features for this task. Even though their methods reported good results, such hand-crafted features are insufficient to separate vehicles from the complex background. Recently, DCNN based methods have achieved great successes in object detection and classification (Krizhevsky et al., 2012; Girshick et al., 2014; Tang et al., 2017; Carlet and Abayowa, 2017) .

Finally, the extracted features are feed to a classifier. Support Vector Machine (SVM) and Random Forest (RF) are two of the most popular classifiers (Zhao and Nevatia, 2003; Gleason et al., 2011; Liu and Mattyus, 2015; Rey et al., 2017) because of their high efficiency and robustness. Until now, they are also employed as the final classifier of some CNN based methods (Girshick et al., 2014). Recently, softmax is the first choice for the classifier of DCNN based methods because it provides normalized probabilistic prediction. Then the cross entropy (CE) is used to calculate the loss for propagation to update the parameters of the network (Le-Cun et al., 2015).

The methods which consist of these three steps are well known as *two-stage* methods: candidate region proposal at the first stage and object classification at the second stage. The CNN based two-stage methods achieve the state-of-the-art performance in terms of accuracy. In contrast, the methods which do not need an additional operation for region proposals, such as YOLO (Redmon et al., 2016) and SSD (Liu et al., 2016), are one-stage-methods. They perform much faster than two-stage methods with compromise of accuracy. Especially, their performance of detecting objects in small scale is very poor. This demerit limits their application

for vehicle detection in aerial images. Therefore, we utilize two-stage method in our framework.

For training a well performing CNN based methods which has millions of parameters, large dataset is the key factor. In the past, some well known large-scale datasets for different tasks are published, *e.g.* ImageNet (Deng et al., 2009) for object classification, Cityscapes dataset (Cordts et al., 2016) for semantic segmentation, *etc.* All of them consists of tens of thousands images for training the model. Even though many existing benchmark datasets contain varieties of vehicles, they are collected in the ground view. These datasets are not applicable to train a framework for vehicle detection in aerial images. There are also existing some well annotated dataset for aerial images, such as the VEDAI dataset (Razakarivony and Jurie, 2016) and DLR 3K dataset (Liu and Mattyus, 2015). However, the objects in the VEDAI dataset are relative easy to detect because of the small number of vehicles which sparsely distribute in the images, and the background is simple. The more challenging and realistic DLR 3K dataset contains totally 20 aerial images with resolution of 5616×3744 . 10 images (3505 vehicles) are used for training. Such number of training samples seems too small for training a CNN model. In comparison with aforementioned datasets, our new dataset ITCVD provides 135 images with 23543 vehicles for training the network.

3. Proposed Framework

An overview of the proposed framework is illustrated in Figure 2. It's modified based on the standard Faster R-CNN (Ren et al., 2015). We refer readers to Ren et al. (2015) for the general procedure of object detection. In this work, we choose ResNet (He et al., 2016) as the backbone structure for feature learning, because of its high efficiency, robustness and effectiveness during training (Canziani et al., 2016).

3.1. Skip Connection

It has been proven in the task of semantic segmentation that, features from the shallower layers retain more detail information (Long et al., 2015). In the task of object detection, the sizes of vehicles in aerial images are ca. 30×50 pixels, assuming 10cm GSD. The size of the output feature maps of the ResNet from the 5th pooling layers is only one 32nd of the input size (He et al., 2016). The shorter edges of most vehicles are very small when they are projected on the feature maps after the 5th pooling layer. So, they will be ignored because their sizes are rounded

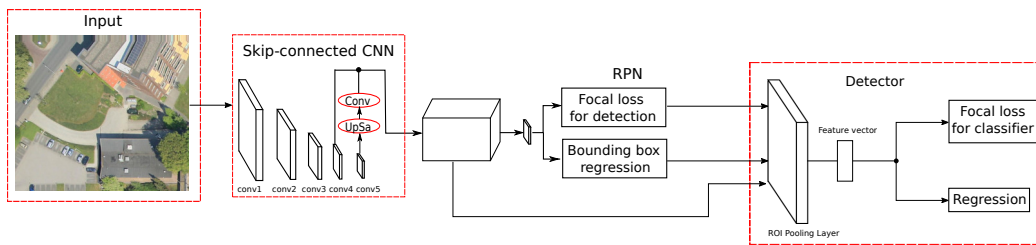


Figure 2: The overview of the proposed framework DFL-CNN. It consists of three main parts: 1) A skip-connection from the low layer to the high layer is added to learn features which contains rich detail information. 2) Focal loss function (Lin et al., 2017) is adopted in the RPN instead of traditional cross entropy. 3) Focal loss function replaces the cross entropy in the classifier.

up. Furthermore, pooling operation leads to significant loss of detailed information. For densely packed area, it is difficult to separate individual vehicles. For example, as shown in Figure 3, the extracted features from the shallow layer (Figure 3b) have richer detailed information than the features from the deeper layer (Figure 3c). In the case of densely packed area (Figure 3a), the detail information play an important to separate the individual vehicles from each other. Therefore,

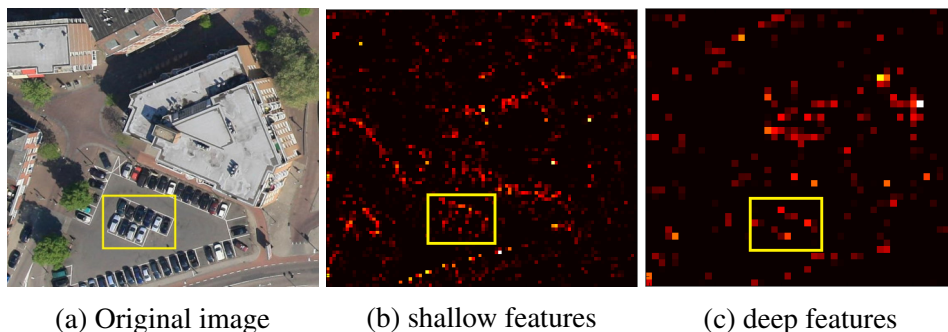


Figure 3: Comparison of the extracted features from the 4th pooling layer (b) and the 5th pooling layer (c). They are illustrated in heat map. The yellow bounding box indicate the corresponding region in the original image and the feature maps.

we fuse the features from the shallow layers, which contain more detail information, with the features learned by deeper layers, which have more representative abilities, to precisely localize detected individual vehicle. This skip-connected CNN architecture is illustrated in Figure 4. The image fed to the network is 752×674 pixels. The size of the feature maps from the 4th and 5th pooling layers are $42 \times 47 \times 1024$ and $21 \times 24 \times 2048$ respectively. To fuse them together, the smaller feature maps are upsampled to the size of $42 \times 47 \times 2048$, and then

reduced the feature channels into 1024 by a 1×1 convolution layer. Then the two feature maps are concatenated as the skip-connected feature maps.

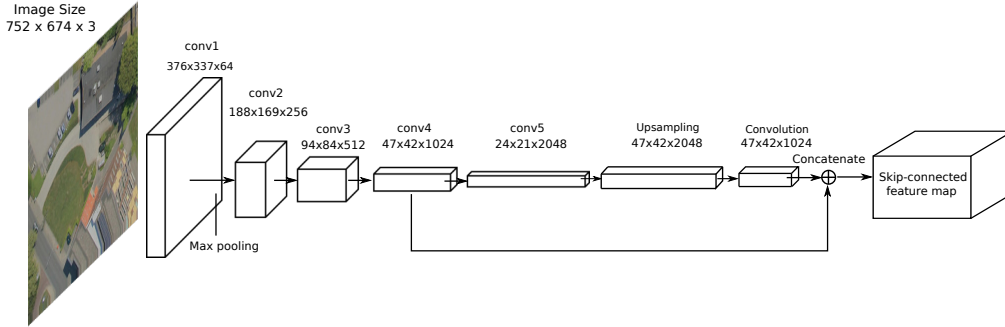


Figure 4: Structure of skip-connected CNN. The feature maps from the conv5 are upsampled to the same size as the feature maps from conv4. Then, the number of the feature channels are reduced by 1×1 convolution layer into 1024. Finally, the feature maps from conv4 and conv5 are concatenated.

3.2. Loss function

Cross entropy (CE) is the most popular loss function used for object classification. It can reduce the imbalance between positive and negative samples. But it is not good enough to train classifier for distinguishing easy and hard classified examples. This problem becomes more significant in the task of vehicle detection in the aerial images because of the monotone appearance of target objects and the complex background. For example, windows on the facade may have very similar appearance as the cars.

Focal loss function is original proposed by Lin et al. (2017) to dedicate the class imbalance problems for the one-stage object detectors, such as YOLO (Redmon et al., 2016) and SSD (Liu et al., 2016). As discussed in the paper, a one-stage detector suffers from the extreme foreground-background class imbalance because of the dense candidates which cover spatial positions, scales, and aspect ratios. A two-stage detector handles this challenge in the first stage: candidates proposal, *e.g.* RPN (Ren et al., 2015), most of the candidates which are likely to be the background are canceled, and then the second stage: classifier works on much sparser candidates. However, in the scenes with dense objects of interest, *e.g.*, the parking cars in Figure 1, even the state-of-the-art candidates proposal method RPN is not good enough to filter the dense proposals in two aspects: 1) many of the

dense proposals cover two vehicles and have high overlap with the ground truth, which makes it hard for the proposal methods to determine whether they are background objects. 2) Too many background objects interfere the training. It is hard to select the negative samples which are very similar as the vehicles to enhance the detector/classifier to distinguish them from the positive samples. Inspired by the idea in Lin et al. (2017), we proposed to use the *focal loss function* instead of the conventional CE loss both in the region proposal and the classification stages, dubbed as *double focal loss-CNN* (DFL-CNN). For better understanding, let’s have a brief review on *focal loss function*.

The traditional CE loss for classification (for convenient discussion, we take the binary classification as example) is formally defined as:

$$L_{CE}(p, y) = -\log(p_t), \quad (1)$$

with $p_t = \begin{cases} p & \text{if } y = 1 \\ 1 - p & \text{otherwise,} \end{cases}$ where p is the predicted probability of given candidate having label +1 and y is its ground truth label and $y \in \{-1, +1\}$.

When add a modulating factor $(1 - p_t)^\gamma$ with tunable focusing parameter $\gamma \geq 0$ to the CE loss, the loss function becomes the so call *focal loss* (FL):

$$L_{FL}(p_t) = -(1 - p_t)^\gamma \log(p_t) \quad (2)$$

The focal loss has two main properties: 1) The loss is unaffected by misclassified examples which have small p_t when the modulating factor is near 1. In contrast, when $p_t \rightarrow 1$, the modulating factor is near 0, which down-weights the loss for well-classified examples. 2) When the focusing parameter γ is increased, the effect of modulating factor is also increased. CE is the special case of $\gamma = 0$. Intuitively, the contribution of the easy examples are reduced while the ones from hard examples are enhanced during the training. For example, with $\gamma = 2$ ¹, the focal loss of an example classified with $p_t = 0.9$ is 1% of the CE loss and 0.1% of it when $p_t = 0.968$. If an example is misclassified ($p_t < 0.5$), its importance for training is increased by scaling down its loss 4 times.

3.3. Double Focal Loss CNN

In our DFL-CNN framework, we add a skip connection to fuse the features from the lower (conv4) and higher (conv5) layers, and adopt focal loss function

¹ γ is set to 2 in our experiments.

both in the RPN layer and the final classification layer to overcome the class imbalance and the easy/hard examples challenges in our task.

As discussed in Section 3.1, the final feature maps are 1/16 of the original images. Therefore, each pixel in the feature maps corresponds an region of 16×16 pixels. To generate candidates proposal, centered on each pixel in the feature maps, 9 anchors in 3 different areas (30^2 , 50^2 , 70^2) and 3 different ratios (1:1, 2:1 and 1:2) are generated on the original input image. Every anchor is labeled as either positive or negative sample based on the Intersection-over-Union (IoU) with ground truth. The IoU is formally defined as: $\text{IoU} = \frac{\text{area}(\text{Proposal} \cap \text{Ground Truth})}{\text{area}(\text{Proposal} \cup \text{Ground Truth})}$, where the numerator is the overlapping area of box of candidate and the ground truth box, and the denominator represents the union of them. The proposals which have the IoU more than 0.7, are labeled as positive samples and the ones whose IoU are smaller than 0.1 are labeled as the negative samples. Other proposals are discarded. All the proposals exceeding the boundary of the image are also discarded. During training, each mini-batch consists of 64 positive samples and 64 negative samples.

The loss function for training the RPN using focal loss is defined as:

$$L_{RPN}(\{p_i\}, \{t_i\}) = \frac{1}{N_{cls}} \sum_i L_{cls-FL}(p_i, p_i^*) + \lambda \frac{1}{N_{reg}} \sum_i p_i^* L_{reg}(t_i, t_i^*) \quad (3)$$

where L_{cls-FL} is the focal loss for classification, as defined in Equation (2) and L_{reg} is the loss for bounding box regression. p_i is the predicted probability of proposal i belonging to the foreground and p_i^* is its ground truth label. N_{cls} denotes the total number of samples and N_{reg} is the total number of positive samples. λ is used to weight the loss for bounding box regression². The smooth L_1 loss function is adopted for L_{reg} as in Ren et al. (2015):

$$L_{reg}(t_i, t_i^*) = f_{smooth}(t_i - t_i^*), \quad (4)$$

with $f_{smooth}(j) = \begin{cases} 0.5j^2 & \text{if } |j| < 1 \\ |j| - 0.5 & \text{otherwise.} \end{cases}$

$t = (t_x, t_y, t_w, t_h)$ is the normalized information of the bounding boxes of the positive sample and t^* is its ground truth. Each of the entries is formally defined

² λ is set to 15 in our experiments. Because the size of final feature maps is 47×42 and totally 128 anchors are chosen, therefore the ratio is ca. 15.

as:

$$\begin{aligned}
t_x &= (P_x - A_x)/A_w, & t_y &= (P_y - A_y)/A_h, \\
t_w &= \log(P_w/A_w), & t_h &= \log(P_h/A_h), \\
t_x^* &= (P_x^* - A_x)/A_w, & t_y^* &= (P_y^* - A_y)/A_h, \\
t_w^* &= \log(P_w^*/A_w), & t_h^* &= \log(P_h^*/A_h),
\end{aligned} \tag{5}$$

where (P_x, P_y) is the center coordinate of the predicted bounding box and (P_w, P_h) is its predicted width and height, and so as the the bounding box information of the anchors $A = (A_x, A_y, A_w, A_h)$. P^* is the ground truth bounding box information.

The RPN layer output a set of candidates which are likely to be the objects of interest, *i.e.* vehicles in this work, and there predicted bounding boxes. Then, the features covered by these bounding boxes are cropped out from the feature maps and go through the region of interest (ROI) pooling layer to get a fix the size of features.

Finally, the final classifier subnet are fed with these features and classify their labels, and predict their bounding boxes further. The loss function of the classifier subnet for each candidate is formally defined as:

$$L_{classifier}(P, T) = L_{cls-FL}(P, P^*) + \lambda_2 P^* L_{reg}(T, T^*) \tag{6}$$

where T is defined as:

$$\begin{aligned}
T_x &= (P_x - A_x)/A_w, & T_y &= (P_y - A_y)/A_h, \\
T_w &= \log(P_w/A_w), & T_h &= \log(P_h/A_h), \\
T_x^* &= (P_x^* - A_x)/A_w, & T_y^* &= (P_y^* - A_y)/A_h, \\
T_w^* &= \log(P_w^*/A_w), & T_h^* &= \log(P_h^*/A_h),
\end{aligned} \tag{7}$$

The P_x , A_x and P_x^* denote the bounding boxes of prediction results, anchors and ground truth. The other subscripts of y , w and h are the same as x . We set $\lambda_2 = 1$ to equal the influence of classification and bounding box prediction. During training, the classifier subnet is trained using positive and negative samples in ratio of 1 : 3, same as the conventional training strategy (Ren et al., 2015).

4. ITCVD Dataset

In this section, we introduce the new large-scale, well annotated and challenging ITCVD dataset. The images were taken from an airplane platform which flied

over Enschede, The Netherlands, in the height of ca 330m above the ground (Slagboom en Peeters, 2017). The images are taken in both nadir view and oblique view, as shown in Figure 5. The tilt angle of oblique view is 45 degrees. The Ground Sampling Distance (GSD) of the nadir images is 10cm.

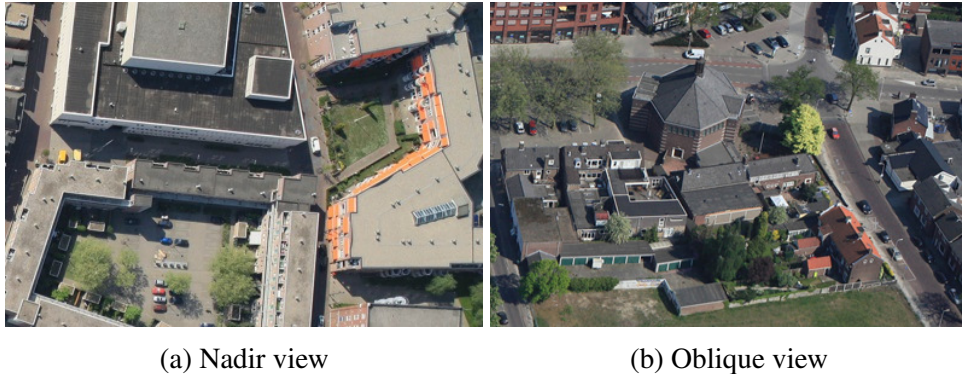


Figure 5: Example images in ITCVD dataset, which are taken in both nadir view (a) and oblique view (b).

The raw dataset contains 228 aerial images with high resolution of 5616×3744 pixels in JPG format. Because the images are taken consecutively with a small time interval, there is ca. 60% overlap between consecutive images. It is important to make sure that, the images used for training do not have common regions with the images that are used for testing. After careful manual selection and verification, 173 images are remained among which 135 images with 23543 vehicles are used for training and the remaining 38 images with 5545 vehicles for testing. Each vehicle in the dataset is manually annotated using a bounding box which is denoted as (x, y, w, h) , where (x, y) is the coordinate of the left-up corner of the box, and (w, h) is the width and height of the box respectively.

5. Experiments

In this section, we discuss about the experimental settings and datasets, in which we evaluate the proposed method and compare with the state-of-the-art object detectors.

5.1. Dataset and experimental settings

We evaluate our method in our ITCVD and DLR 3K datasets (Liu and Matyus, 2015). The statistic information of the two datasets are listed in Table 1. The

state-of-the-art object detector Faster R-CNN (Ren et al., 2015) is implemented in these datasets to provide a strong baseline.

	Training set	Testing set	Image size
ITCVD	135 images (23543 vehicles)	38 images (5545 vehicles)	5616×3744
DLR 3K	10 images (3505 vehicles)	10 images (5928 vehicles)	5616×3744

Table 1: Statistic of ITCVD dataset and DLR 3K dataset (Liu and Mattyus, 2015).

TO save the GPU memory, each original image in the datasets are cropped into small patches uniformly. The resulting new image patches are in the size of 674×752 pixels. The coordinate information of annotation is also updated in the new cropped patches. In the DLR 3K dataset, each vehicle is annotated with a tightly fit bounding box. To adapt our experiment settings, the original annotation is transformed to a normal square bounding box which is expressed with its center point, height and width.

The deep learning models are implemented in Keras with TensorFlow Abadi et al. (2016) backend. The ResNet-50 network He et al. (2016) is used as the backbone CNN structure for feature learning for Faster R-CNN and our model. We use a learning rate of 0.00001 to train the RPN. Note that, other CNN structures, e.g. VGGnet Simonyan and Zisserman (2014) and Google Inception Szegedy et al. (2016), are also applicable in our framework. The CNN structure are pre-trained on ImageNet dataset Deng et al. (2009).

To evaluate the experimental results, the metrics of recall/precision rate and $F1$ -score are used, which are formally defined as:

$$\text{Recall Rate (RR)} = \frac{TP}{TP+FN}, \quad (8)$$

$$\text{Precision Rate (PR)} = \frac{TP}{TP+FP}, \quad (9)$$

$$\text{F1-score} = \frac{2 \times RR \times PR}{RR+PR}. \quad (10)$$

where, TP , FN , FP denote the *true positive*, *false negative* and *false positive* respectively. Furthermore, the relationships between the IoU and RR , PR are also evaluated respectively.

5.2. Results on ITCVD dataset

We evaluated our method DFL-CNN in our challenging ITCVD dataset. The state-of-the-art object detector Faster R-CNN (Ren et al., 2015) is implemented to

provide a strong baseline. In addition, traditional HOG + SVM method Dalal and Triggs (2005) is provided as a weak baseline.

Figure 6 depicts the relationship between recall rate and the precision rate of DFL-CNN, Faster R-CNN and HOG+SVM algorithms with different IoU in the ITCVD dataset. It is obvious that the CNN based methods (DFL-CNN in green curve and Faster R-CNN in red curve) are significantly better than the traditional method (HOG+SVM in black curve). In the relation between recall and precision, our DFL-CNN method also perform better than Faster R-CNN. According to these relationship curves, $IoU = 0.3$ is a good balance point for the following experimental settings, which reports high recall rate and precision at the same time. Note that, it is also a conventional setting in the task of object detection. The quantitative results of these three methods are given in Table 2 (the results are given with $IoU = 0.3$). We can see that, our method outperforms the others.

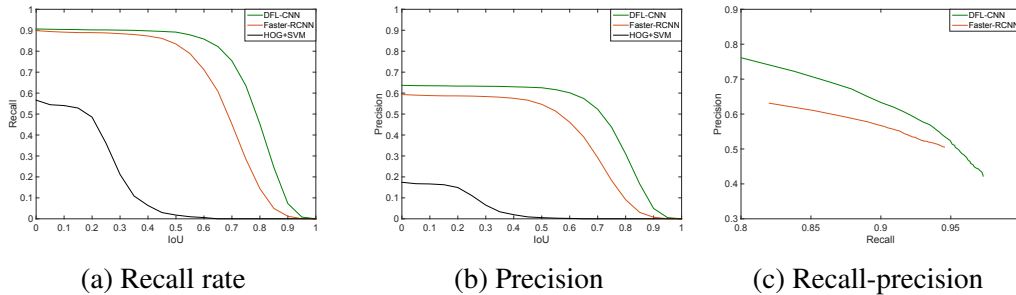


Figure 6: The relationship between IoU and recall rate (a), IoU and precision rate (b) and recall and precision (c) of DFL-CNN, Faster R-CNN, HOG+SVM in the ITCVD dataset respectively.

	HOG+SVM	Faster R-CNN	DFL-CNN
Recall Rate	21.19%	88.38%	89.44%
Precision Rate	6.52%	58.36%	64.61%
F1-score	0.0997	0.7030	0.7502

Table 2: Comparison of baselines and the DFL-CNN method in ITCVD dataset.

To justify the gain by using skip connection and focal loss function, we conducted extensive experiments in ablation studies. First, we train two frameworks both using double focal loss function. But one of the framework has skip connection of the feature maps and the other one not. The qualitative results are shown in Figure 7. We can observe that, the bounding boxes predicted by the framework with skip connection of the feature maps are much more precise than those

that predicted by the framework without skip connection. Individual vehicle is also separated better from others by using the shallow features. Then, we train



Figure 7: Qualitative comparison of bounding box prediction of different frameworks that has no (a) and has (b) skip connection. Other settings are the same.

two frameworks with the skip connection. But one of the framework is trained using CE as loss function and the other using double loss function. The qualitative results are shown in Figure 8. In the results given by CE-trained framework, many background objects that have similar appearances as vehicle are easily to be falsely detected as vehicle. The framework trained using double focal loss function distinguishes these hard negative samples much better from the real vehicles.

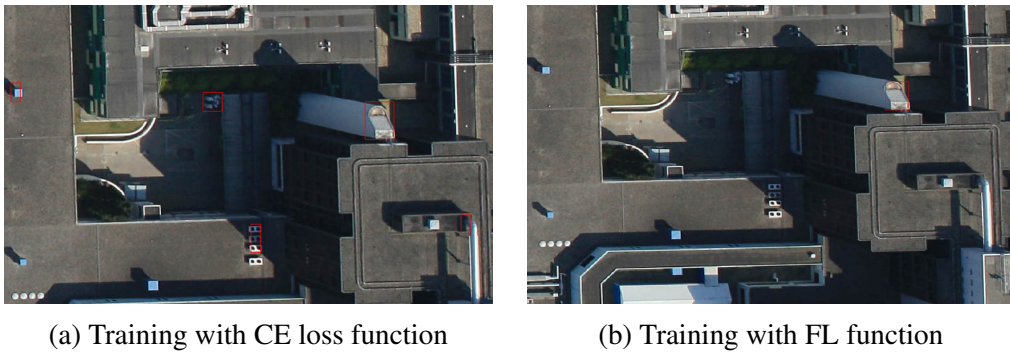


Figure 8: Qualitative comparison of vehicle detection of different frameworks that is trained using CE loss(a) and FL (b) function. Other settings are the same.

Figure 9 gives some examples of bad detection results of the proposed method. Even through our method achieves significant improvements in detection precision and recall rate than the baseline methods, our detector still misses to detect

some obvious vehicles, especially in the crowded parking lot, as shown in Figure 9a. On the other hand, some objects which have very similar appearances as vehicle are also falsely detected, as shown in Figure 9b.

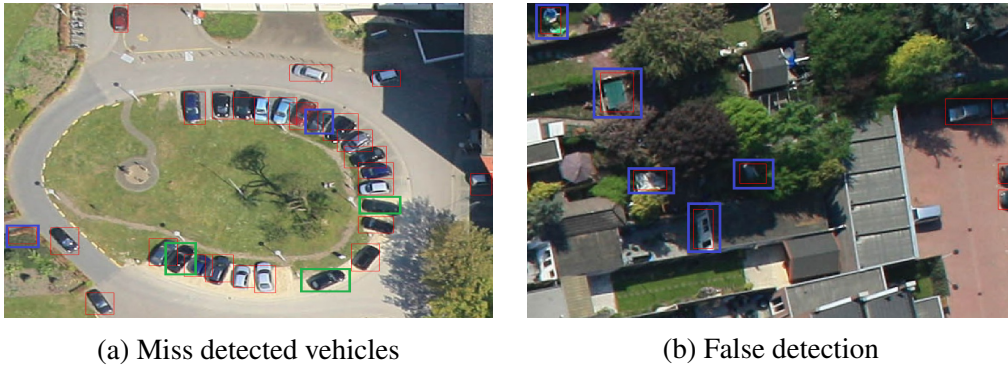


Figure 9: Qualitative examples of incorrect detection by our model. The boxes in red thin line denote the detection results, and the green boxes denote the missed detected vehicles while the blue boxes indicate the false positive prediction.

5.3. Results on DLR 3K dataset

We also evaluated our model in DLR 3K dataset (Liu and Mattyus, 2015). In Figure 10, the relationship between the recall rate and precision is depicted, both for the Faster-RCNN and the proposed method. Figure 10 also indicate that, our method outperform the standard Faster R-CNN in terms of recall rate and precision. In particular, we compared the performance of Faster R-CNN and DFL-

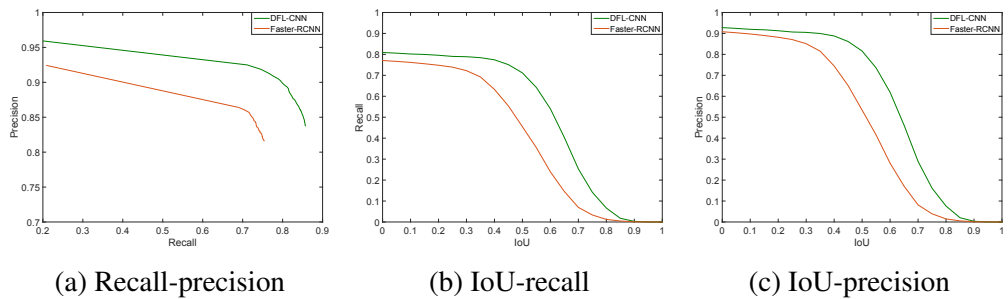


Figure 10: The relationship between recall and precision (a), IoU and precision (b) and IoU and recall rate (c) of DFL-CNN and Faster R-CNN in the DLR 3K dataset (Liu and Mattyus, 2015).

CNN in the case of densely parked vehicles in DLR 3K dataset, as shown in

Figure 11. From the qualitative results we can see that, DFL-CNN (Figure 11b) detected more individual vehicles and predicted more precise bounding boxes than Faster R-CNN (Figure 11a).

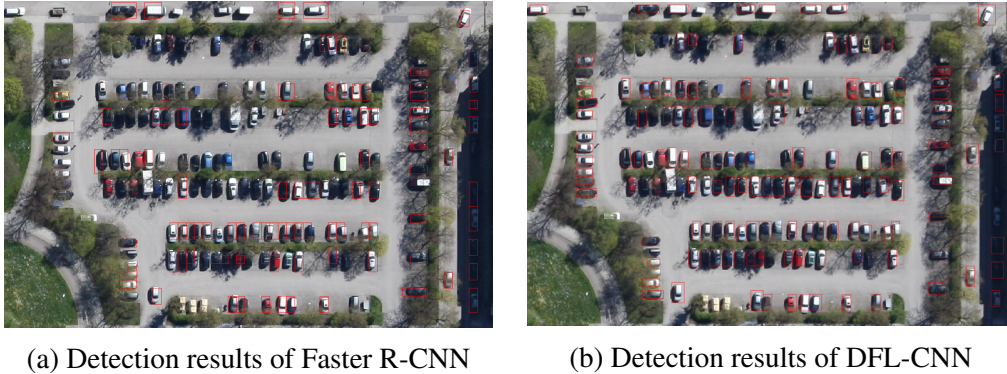


Figure 11: Qualitative comparison of detection results given by Faster R-CNN (a) and DFL-CNN (b) in the DLR 3K dataset, respectively.

6. Conclusion

In this paper, we have proposed a specific framework DFL-CNN for vehicle detection in the aerial images. We fuse the features properties learned in the lower layer of the network (containing more spatial information) and the ones from higher layer (more representative information) to enhance the network’s ability of distinguishing individual vehicles in a crowded scene. To address the challenges of class imbalance and easy/hard examples, we adopt focal loss function instead of the cross entropy in both of the region proposal stage and the classification stage. We have further introduced the first large-scale vehicle detection dataset ITCVD with ground truth annotations for all the vehicles in the scene. Compared to DLR 3K dataset, our benchmark provides much more object instances as well as novel challenges to the community. The experimental results show that our method outperforms the state-of-the-art in these two datasets. For future work, we will extend DFL-CNN to recognize the vehicle types and detect the vehicle orientations. We will also continue to update ITCVD dataset to grow in size and scope. We believe the new ITCVD dataset will promote the development of object detection algorithms in the photogrammetry community.

Acknowledgments

The work is funded by DFG (German Research Foundation) YA 351/2-1 and RO 4804/2-1. The authors gratefully acknowledge the support. We thank Slagboom en Peeters for providing the aerial images.

References

- Abadi, M., Agarwal, A., Barham, P., Brevdo, E., Chen, Z., Citro, C., Corrado, G. S., Davis, A., Dean, J., Devin, M., et al., 2016. Tensorflow: Large-scale machine learning on heterogeneous distributed systems. arXiv preprint arXiv:1603.04467. 5
- Bai, H., Wu, J., Liu, C., 2006. Motion and haar-like features based vehicle detection. In: International Conference on Multi-Media Modelling. pp. 4–pp.
- Caba Heilbron, F., Escorcia, V., Ghanem, B., Carlos Niebles, J., 2015. Activitynet: A large-scale video benchmark for human activity understanding. In: IEEE Conference on Computer Vision and Pattern Recognition. pp. 961–970. 10
- Canziani, A., Paszke, A., Culurciello, E., 2016. An analysis of deep neural network models for practical applications. arXiv preprint arXiv:1605.07678.
- Carlet, J., Abayowa, B., 2017. Fast vehicle detection in aerial imagery. arXiv preprint arXiv:1709.08666.
- 15 Chen, X., Xiang, S., Liu, C.-L., Pan, C.-H., 2014. Vehicle detection in satellite images by hybrid deep convolutional neural networks. IEEE Geoscience and remote sensing letters 11 (10), 1797–1801.
- Chen, Z., Wang, C., Luo, H., Wang, H., Chen, Y., Wen, C., Yu, Y., Cao, L., Li, J., 2016. Vehicle detection in high-resolution aerial images based on fast sparse representation classification and multiorder feature. IEEE Transactions on Intelligent Transportation Systems 17 (8), 2296–2309. 20
- Cheng, H.-Y., Weng, C.-C., Chen, Y.-Y., 2012. Vehicle detection in aerial surveillance using dynamic bayesian networks. IEEE Transactions on Image Processing 21 (4), 2152–2159.

- 25 Cordts, M., Omran, M., Ramos, S., Rehfeld, T., Enzweiler, M., Benenson, R.,
Franke, U., Roth, S., Schiele, B., 2016. The cityscapes dataset for semantic ur-
ban scene understanding. In: IEEE Conference on Computer Vision and Pattern
Recognition.
- Dalal, N., Triggs, B., 2005. Histograms of oriented gradients for human detection.
30 In: IEEE Conference on Computer Vision and Pattern Recognition. pp. 886–
893.
- Deng, J., Dong, W., Socher, R., Li, L.-J., Li, K., Fei-Fei, L., 2009. Imagenet:
A large-scale hierarchical image database. In: IEEE Conference on Computer
Vision and Pattern Recognition. pp. 248–255.
- 35 Felzenszwalb, P. F., Girshick, R. B., McAllester, D., Ramanan, D., 2010. Object
detection with discriminatively trained part-based models. IEEE transactions
on pattern analysis and machine intelligence 32 (9), 1627–1645.
- Girshick, R., 2015. Fast r-cnn. In: IEEE international conference on computer
vision. pp. 1440–1448.
- 40 Girshick, R., Donahue, J., Darrell, T., Malik, J., 2014. Rich feature hierarchies for
accurate object detection and semantic segmentation. In: IEEE Conference on
Computer Vision and Pattern Recognition. pp. 580–587.
- Gleason, J., Nefian, A. V., Bouysounousse, X., Fong, T., Bebis, G., 2011. Vehicle
detection from aerial imagery. In: IEEE International Conference on Robotics
45 and Automation. pp. 2065–2070.
- Han, F., Shan, Y., Cekander, R., Sawhney, H. S., Kumar, R., 2006. A two-stage
approach to people and vehicle detection with hog-based svm. In: Performance
Metrics for Intelligent Systems Workshop. pp. 133–140.
- He, K., Zhang, X., Ren, S., Sun, J., 2016. Deep residual learning for image recog-
50 nition. In: Proceedings of the IEEE conference on computer vision and pattern
recognition. pp. 770–778.
- Kembhavi, A., Harwood, D., Davis, L. S., 2011. Vehicle detection using partial
least squares. IEEE Transactions on Pattern Analysis and Machine Intelligence
33 (6), 1250–1265.

- 55 Krizhevsky, A., Sutskever, I., Hinton, G. E., 2012. Imagenet classification with deep convolutional neural networks. In: *Advances in neural information processing systems*. pp. 1097–1105.
- LeCun, Y., Bengio, Y., Hinton, G., 2015. Deep learning. *Nature* 521 (7553), 436–444.
- 60 LeCun, Y., Boser, B. E., Denker, J. S., Henderson, D., Howard, R. E., Hubbard, W. E., Jackel, L. D., 1990. Handwritten digit recognition with a back-propagation network. In: *Advances in neural information processing systems*. pp. 396–404.
- Lin, T.-Y., Goyal, P., Girshick, R., He, K., Dollár, P., 2017. Focal loss for dense
65 object detection. *arXiv preprint arXiv:1708.02002*.
- Liu, K., Mattyus, G., 2015. Fast multiclass vehicle detection on aerial images. *IEEE Geoscience and Remote Sensing Letters* 12 (9), 1938–1942.
- Liu, W., Anguelov, D., Erhan, D., Szegedy, C., Reed, S., Fu, C.-Y., Berg, A. C.,
70 *Ssd: Single shot multibox detector*. In: *European Conference on Computer Vision*. Springer, pp. 21–37.
- Long, J., Shelhamer, E., Darrell, T., 2015. Fully convolutional networks for semantic segmentation. In: *IEEE Conference on Computer Vision and Pattern Recognition*. pp. 3431–3440.
- Razakarivony, S., Jurie, F., 2016. Vehicle detection in aerial imagery: A small
75 target detection benchmark. *Journal of Visual Communication and Image Representation* 34, 187–203.
- Redmon, J., Divvala, S., Girshick, R., Farhadi, A., 2016. You only look once: Unified, real-time object detection. In: *IEEE Conference on Computer Vision and Pattern Recognition*. pp. 779–788.
- 80 Ren, S., He, K., Girshick, R., Sun, J., 2015. Faster r-cnn: Towards real-time object detection with region proposal networks. In: *Advances in neural information processing systems*. pp. 91–99.
- Rey, N., Volpi, M., Joost, S., Tuia, D., 2017. Detecting animals in african savanna with uavs and the crowds. *Remote Sensing of Environment* 200, 341 – 351.

- 85 Simonyan, K., Zisserman, A., 2014. Very deep convolutional networks for large-scale image recognition. arXiv preprint arXiv:1409.1556.
- Slagboom en Peeters, 2017.
URL <http://www.slagboomenpeeters.com/>
- 90 Szegedy, C., Vanhoucke, V., Ioffe, S., Shlens, J., Wojna, Z., 2016. Rethinking the inception architecture for computer vision. In: Proceedings of the IEEE Conference on Computer Vision and Pattern Recognition. pp. 2818–2826.
- Tang, T., Zhou, S., Deng, Z., Zou, H., Lei, L., 2017. Vehicle detection in aerial images based on region convolutional neural networks and hard negative example mining. *Sensors* 17 (2), 336.
- 95 Uijlings, J. R., Van De Sande, K. E., Gevers, T., Smeulders, A. W., 2013. Selective search for object recognition. *International Journal of Computer Vision* 104 (2), 154–171.
- Xia, G., Bai, X., Ding, J., Zhu, Z., Belongie, S., Luo, J., Datcu, M., Pelillo, M., Zhang, L., 2017. DOTA: A large-scale dataset for object detection in aerial images. CoRR abs/1711.10398.
- 100 Zhao, T., Nevatia, R., 2003. Car detection in low resolution aerial images. *Image and Vision Computing* 21 (8), 693–703.